Available online at www.sciencedirect.com
ScienceDirect
Journal of Power Sources 179 (2008) 252–264
JOURNAL OF POWER SOURCES
www.elsevier.com/locate/jpowsour

Coolant controls of a PEM fuel cell system

Jong-Woo Ahn *, Song-Yul Choe **

Mechanical Engineering Department, Auburn University, Auburn, AL 36848, USA

Received 29 October 2007; received in revised form 6 December 2007; accepted 7 December 2007
Available online 27 December 2007

Abstract

When operating the polymer electrolyte membrane (PEM) fuel cell stack, temperatures in the stack continuously change as the load current varies. The temperature directly affects the rate of chemical reactions and transport of water and reactants. Elevated temperature increases the mobility of water vapor, which reduces the ohmic over-potential in the membrane and eases removal of water produced. Adversely, the high temperature might impose thermal stress on the membrane and cathode catalyst and cause degradation. Conversely, excessive supply of coolants lowers the temperature in the stack and reduces the rate of the chemical reactions and water activity. Corresponding parasitic power dissipated at the electrical coolant pump increases and overall efficiency of the power system drops.

Therefore, proper design of a control for the coolant flow plays an important role in ensuring highly reliable and efficient operations of the fuel cell system.

Herein, we propose a new temperature control strategy based on a thermal circuit. The proposed thermal circuit consists of a bypass valve, a radiator with a fan, a reservoir and a coolant pump, while a blower and inlet and outlet manifolds are components of the air supply system. Classic proportional and integral (PI) controllers and a state feedback control for the thermal circuit were used in the design. In addition, the heat source term, which is dependent upon the load current, was feed-forwarded to the closed loop and the temperature effects on the air flow rate were minimized.

The dynamics and performance of the designed controllers were evaluated and analyzed by computer simulations using developed dynamic fuel cell system models, where a multi-step current and an experimental current profile measured at the federal urban driving schedule (FUDS) were applied. The results show that the proposed control strategy cannot only suppress a temperature rise in the catalyst layer and prevent oxygen starvation, but also reduce the parasitic power dissipated for operation of the air blower and coolant pump.

Keywords: PEMFC; Controls; Thermal circuit; Air supply system; Dynamic modeling

1. Introduction

The PEM fuel cell is a device used to generate electrical power via a chemical reaction whose only byproducts are heat and water. Thus, the fuel cell does not produce air pollution, an advantage that might allow the PEM fuel cell to be considered as a potential alternative energy source for future automotive and stationary applications.

To replace conventional power sources, fuel cell systems must exhibit exceptional performance, efficiency and reliability. Important properties that affect the performance of PEM fuel cells include transport of reactants and byproducts, rejection of the heat generated by electrochemical reactions or by the current passing through the fuel cell and control of humidity to maintain adequate electrolyte conductivity [1].

Balance-of-plant (BOP) is a group of system components that supply reactants, remove the heat generated, remove the water produced and control the actuators. Typical components for operation of a PEM fuel cell system include a hydrogen tank to store fuel, an air compressor or blower along with the inlet/outlet manifolds, a humidifier to supply humidified air, a bypass valve, a radiator with a fan, a reservoir, a coolant pump, several control valves and controllers to reject the heat. A typical configuration is shown in Fig. 1.

As matter of fact, the temperature effects on performance and reliability are one of important issues. When chemical

* Corresponding author. Tel.: +1 334 844 3362.
** Corresponding author. Tel.: +1 344 844 3328; fax: +1 334 844 3307.
E-mail addresses: ahnjong@auburn.edu (J.-W. Ahn), choe@eng.auburn.edu (S.-Y. Choe).

0378-7753/$ – see front matter © 2007 Elsevier B.V. All rights reserved.
doi:10.1016/j.jpowsour.2007.12.066

Nomenclature

A	area (m^2)
b	membrane extension coefficient
C	mass concentration ($kg\,m^{-3}$)
C_p	specific heat ($J\,kg^{-1}\,K^{-1}$)
F	Faraday number ($A\,s\,mol^{-1}$)
F_r	radiator frontal area (m^2)
i	current density ($A\,m^{-2}$)
h	heat transfer coefficient ($W\,m^{-2}\,K^{-1}$)
J	rotational inertia ($kg\,m^2$)
m	mass (kg)
M	molar mass ($kg\,mol^{-1}$)
n	number
N	mole flux ($mol\,s^{-1}\,m^{-2}$)
p	(partial) pressure (Pa)
$\dot{Q}$	heat transfer (W)
R	Universal gas constant ($J\,kg^{-1}\,K^{-1}$)
R	resistance (Ω)
s	entropy ($J\,mol^{-1}\,K^{-1}$)
t	thickness (m)
T	temperature (K)
W	mass flow ($kg\,s^{-1}$)

Subscripts

amb	ambient
an	anode
bl	blower
c	coolant
ca	cathode
catl	catalyst layer
cond	conduction
conv	convection
cv	control volume
diff	diffusion
ele	electro
g	gas
i	index
m	motor
membr	membrane layer
rad	radiator
res	reservoir
s	stator
sou	source
st	stack

Greek symbols

ε	porosity
η	efficiency
λ	water content (ratio)
ρ	density ($kg\,m^{-3}$)
τ	tortuosity, torque (N m)
φ	flux linkage ($V\,s\,rad^{-1}$)
ω	angular velocity ($rad\,s^{-1}$)

reactions occur and transport of charges begins, heat is generated in the cells and temperature rises. The elevated temperature increases the rate of chemical reaction and water activity that affects transport of charges and reactants. However, the temperature should be limited within a working temperature that does not deteriorate material properties of components. When loads for the stack continuously change, the temperature profile in the stack varies and the limit set can be exceeded. The importance of the temperature dynamics was recognized and studied by some authors [2,3] in addition to the temperature effects on reliability of membranes and catalysts. A high working temperature at a given current load increases water flux in the membrane from the anode to the cathode and likely causes dehydration [4]. The rate of Pt particle size growth gets larger at elevated temperature and resulting loss of platinum surface area causes efficiency degradation [5]. Therefore, management of temperature by controlling the coolant flow plays an important role in ensuring highly reliable and efficient operations of the fuel cell system. We have attempted to find a controls law that allows for securing safe and efficient operation of a stack.

2. Models for a PEM fuel cell system

Control of a fuel cell power system requires a better understanding of the dynamic behavior of the stack that interacts with different BOP components. Due to the complexity of the system, dynamic models are used to efficiently design and effectively assess controllers. Models describing the dynamic behavior of the PEM fuel cell stack, air supply and thermal systems are briefly described in the following sections.

2.1. Fuel cell stack

Most fuel cell models describing physical behaviors of a PEM fuel cell are based on either empirical equations whose parameters are obtained by fitting them to the curve of a specific polarization characteristic [6] or the computational fluid dynamics (CFD) that basically solves mass and charge transport in a cell described by using the Navier–Stokes equations [7–9]. The former has been used to design a controller for the air supply system of PEM fuel cell. The lacking dynamics of a fuel cell can be improved by reflecting the charging and discharging behavior of the double layer present on the interface between electrodes and electrolytes. However, such models do not include the gas and temperature dynamics occurring through the flow paths and in the cell when the current is applied. In addition, the partial pressures of reactants drop along the pores in the gas diffusion layer (GDL) that affect the net pressure exerted on the chemical reaction rate and increase the over-potential, are not considered. The temperature rise that eases water removal, increases the chemical reaction and subsequently affects the output voltage of a cell has not been taken into account in this model.

On the other hand, the CFD-based models have been widely used to analyze transport mechanisms of the mass and charge

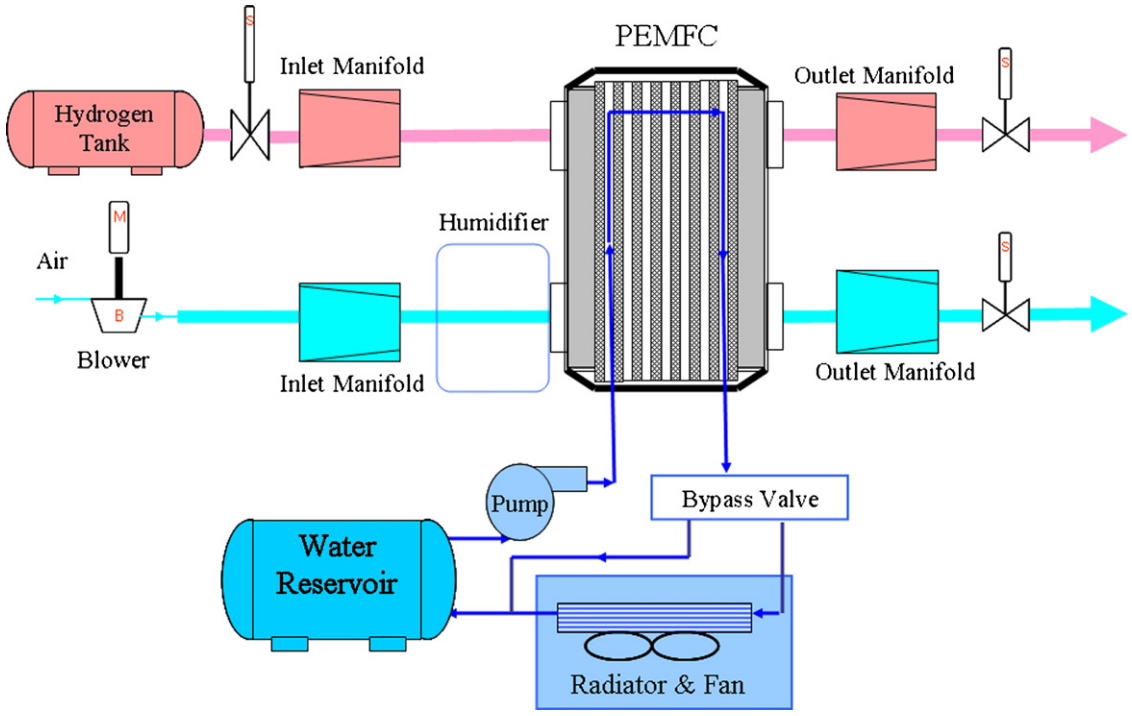

Fig. 1. A schematic diagram of a PEM fuel cell system.

and their spatial distributions in a single cell, but are limited in their ability to represent the dynamic characteristics of a stack for control purposes. In addition, exponential growth of computational time required for unsteady analyses impedes application of the model for design of controls.

Our model was devised on the basis of empirical equations and takes three additional major factors into account: membrane water balance, diffusion in the GDL and temperature distribution.

A PEM fuel cell is constructed by connecting individual models for layers. The *I–V* characteristic is the difference between the open circuit voltage and the over-potentials, which include the ohmic losses in the membrane, the activation over-potential in the catalyst layer on the cathode side and the concentration over-potential. The relationship for a single cell may be written as a function of the physical parameters like the reactant partial pressure, temperature, current and membrane water content [6]. The output characteristic of a stack is assumed to be a multiple of a single cell characteristic and given as follows.

$$V_{\text{cell}} = E(p,T) - v_{\text{act}}(p,T,i) - v_{\text{ohmic}}(i,\lambda_{\text{membr}},T) - v_{\text{conc}}(p,T,i) \quad (1)$$
$$V_{\text{st}} = nV_{\text{cell}}$$

The dynamics of a fuel cell system involve mass flows of air and water. The air supplied flows through the gas flow channel and the GDL before reaching the catalyst layer, and at the same time, takes up water from the humidifier. Water generated in the catalyst layer diffuses through the membrane where protons take water from the anode to the cathode side. The heat generated by the chemical reaction and charge transport raises the temperature in the cell. All of these changes affect the dynamic behavior of the cell. Fuel cell dynamics can be improved by manipulating three factors: (1) water dynamics in the membrane, (2) the partial pressure of oxygen drop in the GDL and (3) temperature variation.

Membrane water content determines proton conductivity. The dynamics of water content are described by the electro-osmotic driving force due to the different electrochemical potentials at the anode and cathode, and the diffusion caused by the water concentration gradient at the two boundaries [10]. Considering the water mass that flows at the boundaries of the membrane layer, the dynamics of the water concentration in the membrane can be improved as follows [11], where C is the mass concentration (kg m^{-3}), M is the mole mass (kg mol^{-1}), b is the membrane extension coefficient [10], ρ is the membrane dry density (kg m^{-3}) and A_{cell} is the fuel cell area (m^2).

$$\lambda_{\text{membr}} = \frac{C_{\text{H}_2\text{O,mass}}/M_{\text{H}_2\text{O}}}{\rho_{\text{dry,membr}}/M_{\text{membr}} - bC_{\text{H}_2\text{O,mass}}/M_{\text{H}_2\text{O}}}$$
$$\dot{m}_{\text{water,membr}} = \frac{\text{d}\left(C_{\text{H}_2\text{O,mass}}A_{\text{cell}}t_{\text{membr}}\right)}{\text{d}t} \quad (2)$$
$$= W_{\text{ele,membr,an}} - W_{\text{ele,membr,ca}} + W_{\text{diff,membr,an}} + W_{\text{diff,membr,ca}}$$

The electro-osmotic driving force created by the different electrochemical potential at the anode and cathode determines the water mass flows of $W_{\text{ele,membr,an}}$ and $W_{\text{ele,membr,ca}}$ at the boundaries of the membrane layer. In addition, the diffusion caused by the water concentration gradient at the two boundaries makes up the mass flows of $W_{\text{diff,membr,an}}$ and $W_{\text{diff,membr,ca}}$.

Those relationships are described by Eqs. (3)–(5) proposed by Springer [10].

$$n_{\mathrm{d}} = 0.0029\lambda_{\mathrm{membr}}^2 + 0.05\lambda_{\mathrm{membr}} - 3.4 \times 10^{-19} \tag{3}$$

$$W_{\mathrm{ele,membr},i} = M_{\mathrm{water}} A_{\mathrm{cell}} n_{\mathrm{d},i} \frac{i}{F} \tag{4}$$

$$W_{\mathrm{diff,membr},i} = M_{\mathrm{water}} A_{\mathrm{cell}} D_{\mathrm{water}} \frac{(C_i - C_{\mathrm{mid}})}{t_{\mathrm{membr}}} \tag{5}$$

where the diffusion coefficient D_{water} and the water concentration C_i are calculated from the empirical equations [10] expressed as a function of membrane water content λ_{membr}.

$$D_{\mathrm{water}} = D(\lambda_{\mathrm{membr}}) \exp\left(2416\left(\frac{1}{303} - \frac{1}{T_{\mathrm{membr}}}\right)\right) \tag{6}$$

$$D(\lambda_{\mathrm{membr}}) = \begin{cases} 10^{-6} & 2 > \lambda_{\mathrm{membr}} \\ 10^{-6}(1 + 2(\lambda_{\mathrm{membr}} - 3)) & 3 \geq \lambda_{\mathrm{membr}} \geq 2 \\ 10^{-6}(3 - 1.67(\lambda_{\mathrm{membr}} - 3)) & 4.5 > \lambda_{\mathrm{membr}} > 3 \\ 1.25 \times 10^{-6} & \lambda_{\mathrm{membr}} \geq 4.5 \end{cases} \tag{7}$$

The boundary water content λ_i is a function of water activity a_i, which is calculated from the water vapor partial pressure

$$\lambda_i = \begin{cases} 0.043 + 17.81a_i - 39.85a_i^2 + 36a_i^3 & 1 \geq a_i > 0 \\ 14 + 1.4(a_i - 1) & 3 \geq a_i > 1 \\ 16.8 & a_i \geq 3 \end{cases} \tag{8}$$

$$a_i = \frac{P_{v,i}}{P_{\mathrm{sat},i}} \tag{9}$$

The reactant entering the cell diffuses through the GDL before reaching the catalyst layer, and significantly affects the overall dynamics of the reactants. This diffusion effect is described by using the mass continuity and the Stefan–Maxwell Eq. (10) [12]:

$$\begin{aligned} &\frac{\varepsilon_{\mathrm{g}}}{RT}\frac{\partial p_i}{\partial t} + \frac{\partial N_i}{\partial y} = 0 \\ &\frac{\varepsilon_{\mathrm{g}}}{\tau^2}\frac{\partial p_i}{\partial y} = \sum_{k=1}^{3} \frac{RT}{p_{ca} D_{ik}} (p_i N_k - p_k N_i) \end{aligned} \tag{10}$$

Hence, $i, k \in (1, 3)$ represents the sum of the species partial pressures, where p_1 is the oxygen partial pressure, $p_2 = P_{\mathrm{sat}}(T)$ and p_3 are the water vapor and the nitrogen partial pressures, respectively, and the diffusion coefficients of $p_{\mathrm{ca}} D_{ik}$ include the cathode pressure of p_{ca}. The parameters ε_{g} and τ are the porosity and the tortuosity of the GDL.

If a cell assembled with cubical layers is isotropic and constant, then the energy conservation equation can be applied. Accordingly, the total energy change in a controlled volume is equal to the sum of the energy exchanged at the boundaries of a control volume and internal energy resources. In fact, the energy exchanged at the boundaries occurs in two ways: (a) conduction across the cell and (b) convection occurring between bipolar plates with the coolant, reactants and water. Thus, the thermal-dynamic behavior can be described using the following energy conservation Eq. (11) [11]:

$$\begin{aligned} \sum_i C_{p_i} C_{i,\mathrm{mass}} A_{\mathrm{cell}} t_{\mathrm{cv}} \frac{\mathrm{d}T_{\mathrm{cv}}}{\mathrm{d}t} &= \underbrace{\sum W_{\mathrm{in}} C_{p_j} (T_{\mathrm{in}} - T_{\mathrm{cv}})}_{\text{mass flow in}} + \underbrace{\dot{Q}_{\mathrm{conv}}}_{\text{convection heat transfer}} \\ &+ \underbrace{\dot{Q}_{\mathrm{cond}}}_{\text{conduction heat transfer}} + \underbrace{\dot{Q}_{\mathrm{sou}}}_{\text{sources}} \end{aligned} \tag{11}$$

The internal energy source is composed of the entropy loss and the chemical energy required for protons to overcome the barrier of the over-potentials in both catalyst layers (12). In addition, other source terms are ohmic losses caused by transport of electrons and protons in the cell [13]:

$$\dot{Q}_{\mathrm{sou}} = I\left(-\frac{T\Delta s}{4F} + v_{\mathrm{act}} + IR_{\mathrm{membr}}\right) \tag{12}$$

where Δs is equal to -326.36 (J mol^{-1} K^{-1}) [14], v_{act} is given in the reference [15] and R_{membr} is the membrane resistance.

2.2. Air supply system

The air supply system consists of four subsystems; an air supplier, a humidifier and an inlet and outlet manifolds with a regulator adjusting the pressure at the stack. It functions to continuously replenish the air to the fuel cell stack as the load varies. As an air supplier, a compressor or a blower are widely employed. One of the advantages for the use of a blower is the less consumption of the parasitic power than that of the compressor and consequently overall efficiency of the system can be augmented [16]. The blower is connected between a humidifier and inlets of flow channels via pipes. The humidifier described here is simplified as the ideal, with no associated dynamics or energy losses. The blower is usually driven by an electric motor. The dynamic characteristics of the blower system can be described by the sum of all moments of inertia of the motor and the impeller, and the torque produced by the motor. Hence, the torque produced by the motor, $\tau_{\mathrm{bl,m}}$ (J), is a function of the stator resistance, $R_{\mathrm{s,bl,m}}$ (Ohm), flux linkage, $\Phi_{\mathrm{bl,m}}$ (V s rad^{-1}) and the number of the poles, $n_{\mathrm{bl,m,pl}}$, with the stator voltage, $V_{\mathrm{bl,m}}$ (V) [17].

$$\begin{aligned} \frac{\mathrm{d}\omega_{\mathrm{bl}}}{\mathrm{d}t} &= \frac{1}{J_{\mathrm{bl}}}\left(\tau_{\mathrm{bl,m}} - \frac{W_{\mathrm{bl}} \Delta P_{\mathrm{bl}} \eta_{\mathrm{bl,m}}}{\eta_{\mathrm{bl}} \rho_{\mathrm{amb}} \omega_{\mathrm{bl}}}\right) \\ \tau_{\mathrm{bl,m}} &= \eta_{\mathrm{bl,m}} \frac{3}{2} \frac{\eta_{\mathrm{bl,m,pl}}}{2} \frac{\Phi_{\mathrm{bl,m,pl}}}{\eta_{\mathrm{s,bl,m}}} \left[V_{\mathrm{bl,m}} - \left(\frac{N_{\mathrm{bl,m,pl}}}{2}\right) \Phi_{\mathrm{bl,m}} \omega_{\mathrm{bl}}\right] \end{aligned} \tag{13}$$

where ω is the angular velocity (rad s^{-1}), J is the rotational inertia (kg m^2), η is the efficiency, p is the pressure (Pa) and ρ is the air density (kg m^{-3}). The air blower flow rate is a function of the angular velocity and pressure, and the efficiency is a function

of the flow rate and the angular velocity [17].

$$W_{\mathrm{bl}} = \begin{cases} \omega_{\mathrm{bl}}(-20.581 \times (p^*)^2 - 1.4415 \times 10^{-3} \times p^* \\ \quad +4.1333 \times 10^{-5}),\ p^* \le 9 \times 10^{-4}\ \mathrm{Pa\,s^2\,rad^{-2}} \\ \text{otherwise}, \quad \omega_{\mathrm{bl}}(-1.7973 \times p^* + 1.6409 \times 10^{-3}) \end{cases} \tag{14}$$

$$\eta_{\mathrm{bl}} = -2.8831 \times 10^{13} \times \left(\frac{W_{\mathrm{bl}}}{\omega_{\mathrm{bl}}}\right)^3 + 9.5115 \times 10^{8} \times \left(\frac{W_{\mathrm{bl}}}{\omega_{\mathrm{bl}}}\right)^2 + 1.3087 \times 10^{4} \times \left(\frac{W_{\mathrm{bl}}}{\omega_{\mathrm{bl}}}\right) + 0.17945 \tag{15}$$

where p^* is $(p_{\mathrm{ca}} - p_{\mathrm{amb}}/\omega_{\mathrm{bl}}^2)$.

The blower parameters are extracted by characteristic data and specifications as provided by PADT (Phoenix Analysis & Design Technologies) [18], which includes both the flow parameter and overall efficiency versus the head parameter.

Dynamic characteristics of the inlet and outlet manifold pressures are described by using the mass conservation equation.

$$\frac{\mathrm{d}p_{\mathrm{im}}}{\mathrm{d}t} = \frac{\gamma R_{\mathrm{a}}}{V_{\mathrm{im}}}(W_{\mathrm{bl}} T_{\mathrm{bl}} - W_{\mathrm{im,out}} T_{\mathrm{im}}) \tag{16}$$

2.3. Thermal circuit

A thermal circuit should dissipate the heat produced by the stack. The circuit has 3 components including a three-way valve to allow the coolant to bypass, a radiator to exchange heat with the ambient media, a fan to increase the effectiveness of heat convection and a reservoir to store the coolants. A coolant pump supplies the coolant for the heat source.

The opening width of the bypass valve is assumed to be linear with a factor k. Then, the coolant temperature at the reservoir inlet, $T_{\mathrm{res,c,out}}$, can be expressed as a function of the stack outlet, $T_{\mathrm{st,c,out}}$, and the radiator outlet, $T_{\mathrm{rad,c,out}}$ and k.

$$W_{\mathrm{c}} C_{p_{\mathrm{c}}} T_{\mathrm{res,c,in}} = (1-k) W_{\mathrm{c}} C_{p_{\mathrm{c}}} T_{\mathrm{st,c,out}} + k W_{\mathrm{c}} C_{p_{\mathrm{c}}} T_{\mathrm{rad,c,out}} \tag{17}$$

The behavior of the radiator follows thermodynamic principles Kroger [19] proposed an empirical equation for the heat transfer coefficient of the radiator, h_{rad} ($\mathrm{k\,W m^{-2}\,K^{-1}}$) and pressure drop, p_{r} (kPa) of the radiator as a function of the air flow rate, W_{air} ($\mathrm{kg\,s^{-1}}$) [13].

$$\begin{aligned} h_{\mathrm{rad}} &= -1.4495 W_{\mathrm{air}}^2 + 5.9045 W_{\mathrm{air}} - 0.1157 \\ p_{\mathrm{r}} &= (326.12 W_{\mathrm{air}} - 75.396) + 101.325 \end{aligned} \tag{18}$$

If the heat of the coolant is transferred completely to the radiator without any loss, the heat capacity of the coolant is identical to that of the radiator. Thus, the radiator outlet coolant temperature can be expressed as a function of the radiator geometry and the heat convection caused by the temperature difference between the ambient and the radiator outgoing air temperature [13].

$$T_{\mathrm{rad,c,out}} = T_{\mathrm{rad,c,in}} - 0.46\left(\frac{\mathrm{Fr}(T_{\mathrm{rad,c,in}} - T_{\mathrm{amb}})h_{\mathrm{rad}}}{W_{\mathrm{c}} C_{p_{\mathrm{c}}}}\right) \tag{19}$$

Hence, Fr denotes the frontal area ($\mathrm{m^2}$) of the radiator, and $T_{\mathrm{rad,c,in}}$ denotes the radiator inlet coolant temperature (K). The electric power for the fan can be calculated according to a thermal dynamic relationship between the pressure drop and the air flow rate [13],

$$P_{\mathrm{fan}} = \frac{1}{\eta_{\mathrm{elec}}\eta_{\mathrm{fan}}}(W_{\mathrm{air}} C_{p_{\mathrm{air}}} T_{\mathrm{amb}}[P_r^{(k-1/k)} - 1]) \tag{20}$$

where P_{fan} denotes the electric power (W) of the fan.

The reservoir stores the coolants after a heat exchange at the radiator by convection. The variation of the heat in the reservoir is the sum of the heat that the coolant carries and the heat exchanged with the ambient. Therefore, the reservoir outlet coolant temperature at the end of the given time interval, $T_{\mathrm{res,c,out}}$ (K), can be expressed by the equation [13]

$$T_{\mathrm{res,c,out}} = T_{\mathrm{res,p}} - \frac{\Delta t}{m_{\mathrm{res}} C_{p_{\mathrm{res}}}}(W_{\mathrm{c}} C_{p_{\mathrm{c}}}(T_{\mathrm{res,p}} - T_{\mathrm{res,c,in}}) + h_{\mathrm{res}} A_{\mathrm{res}}(T_{\mathrm{res,c,in}} - T_{\mathrm{amb}})) \tag{21}$$

where $T_{\mathrm{res,p}}$ is the temperature (K) of the reservoir at the previous of time point, Δt is the time interval (s), m_{res} is equivalent to the coolant mass in the reservoir (kg), $T_{\mathrm{res,c,in}}$ is the reservoir inlet coolant temperature (K) and h_{res} is the convective heat transfer coefficient of reservoir to the ambient temperature ($\mathrm{W\,m^{-2}\,K^{-1}}$), respectively.

Assuming that all of the heat generated in the stack is completely transferred to the coolant; the coolant flow rate is expressed by its relationship with the heat source [13].

$$W_{\mathrm{c}} = \frac{\dot{Q}_{\mathrm{sou}}}{C_{p_{\mathrm{c}}}\Delta T} \tag{22}$$

At equilibrium, the excessive heat rejected by the coolants is identical to the sum of the heat the reservoir stores and that which the radiator exchanges with the ambient environment. If a maximum coolant flow rate is assumed then the temperature drop along the coolant flow channel can be calculated by considering that the maximum heat produced in the stack should be the same as the amount of heat carried by the coolant flow rate. The temperature at the outlet of the coolant is assumed to be 345.15 K because the temperature gradient from the catalyst to the coolants channel is 8 K at a maximum load current if the catalyst temperature is 353.15 K. Thus, the inlet temperature is obtained at a temperature drop of 12 K and a maximum flow rate of $3\,\mathrm{kg\,s^{-1}}$. The heat transfer coefficient of the radiator and the volume of the reservoir were chosen on the basis of the maximum heat capacity stored and dissipated.

3. Control strategies

Fig. 2 depicts a block diagram of the air supply system and thermal circuit with either PI controllers or state feedback controller.

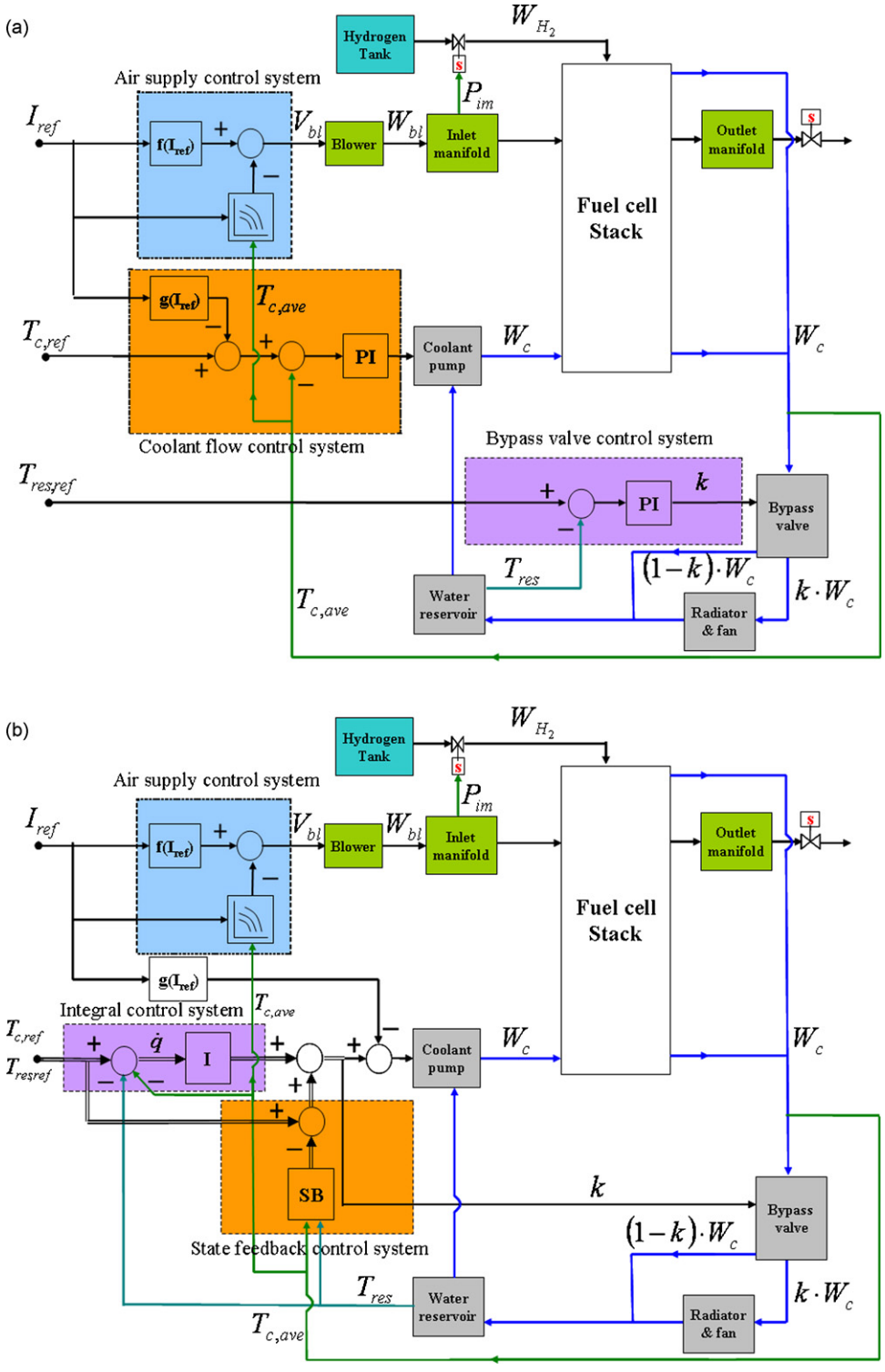

Fig. 2. Block diagram for an air and coolant control with (a) classic PI controllers and (b) state feedback controller with integral controller.

The feedback loop of the air supply system should maintain the optimal oxygen ratio and prevent oxygen starvation that might occur during abrupt changes in the load current. Hence, the oxygen excess ratio is defined as the rate of oxygen supplied to that consumed. While the amount of oxygen consumed depends on the stack current, the amount of oxygen supplied to a fuel cell is directly related to the blow motor voltage. Thus, the air supply controller, a static feed-forward controller (sFF) [20], uses a polynomial that interpolates map data and includes an optimal relationship between the stack current required and the motor voltage of the blower in order to maintain the oxygen ratio at 2. In this case, the air flow of the blower can simply be controlled by the blower motor voltage. The design of this type of controller has extensively reviewed by other authors [21–23].

As shown in Fig. 6, the rejection behavior of the oxygen excess ratio at an occurrence of a temperature rise can be optimized by the controllers.

The stack is regarded as a single thermal mass with a heat capacity. Under the assumption that the heat exchange by radiation and convection to the ambient is negligible, and the stack temperature is equal to the average of the stack outlet coolant temperatures on the anode and cathode side, the variation of the temperature in the stack is equal to the sum of the heat source terms in the stack, the heat exchanged with the coolants.

$$m_{st}C_{p_{st}}\frac{dT_{st}}{dt} = \dot{Q}_{sou} + W_c C_{p_c}(T_{c,in} - T_{st}) \tag{23}$$

where $m_{st}C_{p_{st}}$ is the heat capacity of the stack (J K^{-1}), W_c is the coolant flow rate (kg s^{-1}), the control variable and $\dot{Q}_{sou}$ is the internal energy source (J s^{-1}), a function of the load current.

Due to the nonlinearity of the equations in the lumped thermal stack (Eq. (23)) and the reservoir model (Eq. (21)), Talyor's expansion is used for linearization at an operating point, where the reservoir temperature and coolant flow rate are set at 337.15 K and 0.96 kg s^{-1}, respectively. The stack current and voltage are 140 A and 198 V, respectively. The state equations and variables are defined as follows:

$$\begin{aligned} \delta\dot{x} &= A\delta x + B_u u + B_w w \\ \delta y &= C\delta x \end{aligned} \tag{24}$$

$$\begin{aligned} x &= \begin{bmatrix} T_{st} & T_{res} \end{bmatrix} \quad \text{(states)} \\ u &= \begin{bmatrix} W_c & k \end{bmatrix} \quad \text{(controlled input)} \\ w &= I_{st} \quad \text{(disturbance)} \\ y &= \begin{bmatrix} T_{st} & T_{res} \end{bmatrix} \quad \text{(output)} \end{aligned}$$

where the matrices of the linearized system, A, B_u, B_w and C are listed in the Appendix A.

3.1. Design of classic PI controls

The state equations derived above present a multi-input-multi-output structure, where two controlled input variables, coolant flow rate and bypass valve opening factor, are dependent on each other. This dependence can be minimized if the time constants of two feedback loops are set in a different order. In that case, the temperature in the stack can be controlled by the coolant flow rate independent of the temperature of the coolant being controlled by the opening factor k. Eq. (23) includes a relationship between the stack temperature and the coolant flow rate, whose transfer function is given in Eq. (25). The system follows the first order of an ordinary differential equation and thus a classic PI controller is employed. The two gains of the PI controller are selected by the bandwidth of the closed-loop that is 3 times higher than the time constant of the heat source term response and a damping ratio of 0.707. The resulting gains are $K_{p,c} = 0.25$ and $K_{I,c} = 0.017$ (s^{-1}).

$$\frac{T_{st}(s)}{W_c(s)} = \frac{Cp_c \cdot (T^o_{res} - T^o_{st})}{(m_{st}Cp_{st} \cdot s + W^0_c \cdot Cp_c)} \tag{25}$$

$$G_{c1}(s) = K_{p,c} + \frac{K_{I,c}}{s} \tag{26}$$

Eq. (21) describes the relationship between the temperature in the reservoir and the factor for the bypass valve opening, which the transfer function is given in Eq. (27). Likewise, the gains for the PI controller are selected so that the bandwidth of the closed-loop is 5 times higher than the time constant of the coolant flow feedback outer loop. In addition, the damping ratio is set to 0.707. The resulting gains are $K_{p,b} = 0.1902$ and $K_{I,b} = 0.0546$ (s^{-1}).

$$\frac{T_{res}(s)}{k(s)} = \frac{(W^0_c Cp_c + h_{res}A_{res})(T_{amb} - T^0_{st})}{(m_{res}Cp_{res}s + W^0_c Cp_c)} \tag{27}$$

$$G_{c2}(s) = K_{p,b} + \frac{K_{I,b}}{s} \tag{28}$$

3.2. Design of state feedback controls with integral controls

The parasitic power dissipated in the coolant pump is not considered as a control object by designing the classic PI controller, even though it can reject sufficient amounts of heat and effectively suppresses temperature surges in the layers of the cell. One alternative is the use of a state feedback control, where the parasitic power dissipated in the coolant pump can be considered to be one of the control objectives. On the other hand, the parasitic power of the coolant pump is directly proportional to the coolant flow rate. Thus, the coolant flow rate is included as a parameter in the cost function given below. Optimization of the gains is achieved by the LQR (linear quadratic regulator) method, which sums the square of the errors [24].

$$J = \int_0^\infty (\delta x^T Q_x \delta x + \delta u^T R \delta u)dt \tag{29}$$

Q_x represents the weighting matrix, which amplifies the errors of the control objects, while the other weighting matrix R is used to suppress the effect of manipulating the variables.

The state equation of the control plant presents a 2-by-2 matrix, where the variables are coupled with each other. A decoupling of the two loops has been accomplished by assigning different time constants to the two closed loops. In fact, the valve opening factor does not directly affect the dynamics of the stack temperature, while the reservoir temperature is strongly influenced by the valve opening factor rather than the coolant flow rate. Hence, the time constant of the transfer function between the stack temperature and coolant flow rate is 5 times faster than that between the stack temperature and the valve opening factor.

On the other hand, integrators are required to suppress any steady state errors. Thus, the errors of both closed loops are defined as a new state variable that is considered in the cost function;

$$\dot{q} = \begin{bmatrix} T^*_{st} - T_{st} \\ T^*_{res} - T_{res} \end{bmatrix} \tag{30}$$

$$J = \int_0^\infty (\delta x^{\mathrm{T}} Q_x \delta x + q^{\mathrm{T}} Q_{\mathrm{I}} q + \delta u^{\mathrm{T}} R \delta u)\mathrm{d}t \tag{31}$$

where Q_{I} is the weighting matrix for integrator.

The rules for the optimal control inputs are obtained [25];

$$\delta u = -K\begin{bmatrix}\delta x & q\end{bmatrix}^{\mathrm{T}} = -K_{\mathrm{p}} \cdot \delta x - K_{\mathrm{I}} \cdot q \tag{32}$$

where the controller gain is $K = R^{-1}\mathrm{Bu}'^{\mathrm{T}}\mathrm{P}$. P is the solution of the Algebraic Riccati equation that is given as follows:

$$PA' + A'P + Q - PB'_{\mathrm{u}}R^{-1}B'^{T}_{\mathrm{u}}P = 0 \tag{33}$$

where A', B'_{u}, $Q = \mathrm{diag}(Q_x, Q_{\mathrm{I}})$ and R is listed in Appendix A.

When the weighting matrix R is larger than the weighting matrix Q, the role of the coolant flow rate in the cost function increases, and subsequently, the gains of the controller are chosen, which minimizes the parasitic power. After several iterations with different weighting factors, the optimal control matrix K_{p} and K_{I} is given by

$$K_{\mathrm{p}} = \begin{bmatrix} -1.2015 & 0.01 \\ -0.0521 & -3.1479 \end{bmatrix}, \quad K_{\mathrm{I}} = \begin{bmatrix} -0.1 & 0.0027 \\ -0.0027 & -0.1 \end{bmatrix} \tag{34}$$

3.3. Disturbance compensation

The heat produced in the stack tends to follow the current drawn from the stack. The current-dependent heat is regarded as a disturbance in the control loop. This cannot be fully rejected by the typical coolant control, which measures the temperature at the outlet of the coolants. As a result, the heat dissipated is less than the heat produced. A countermeasure is to estimate the temperature rise in a layer that is directly related to the magnitude of the current load and feed-forward it to the temperature control loop shown in Fig. 2. The relationship between the current and the stack temperature is derived by using Eqs. (12) and (23) yielding the following transfer function (Eq. (35)):

$$\begin{aligned} \frac{T_{\mathrm{st}}(s)}{I(s)} &= \frac{(-T\Delta s/4F + v_{\mathrm{act}})}{(m_{\mathrm{st}}Cp_{\mathrm{st}} \cdot s + Cp_{\mathrm{c}}W_{\mathrm{c}}^0)} \\ \frac{T_{\mathrm{st}}(s)}{I^2(s)} &= \frac{R_{\mathrm{membr}}}{(m_{\mathrm{st}}Cp_{\mathrm{st}} \cdot s + Cp_{\mathrm{c}}W_{\mathrm{c}}^0)} \end{aligned} \tag{35}$$

However, all previously published air supply control designs assumed a constant stack working temperature [20–23]. In fact, distribution of the temperatures in the individual layers through the plane varies because of the various sources of energy occurring in the chemical reactions, and Joule's losses associated with charge transport. In order to dissipate the heat in the stack, the temperature of the coolant control loop is set lower than that in the stack, thereby changing the temperature in the gas flow channels. When the temperature in the channel is lower, the pressure drops according to the ideal gas law for the given volume, and then a pressure difference to the inlet manifold becomes larger. On the other hand, the mass flow rate at the inlet of the stack increases according to the nozzle equation [6] and the oxygen excess ratio increases. The surplus air is reduced by an additional element in the controls that depends upon the coolant temperature in addition to the current that determines the amount of oxygen consumed. However, the relationship between the load current and temperatures given as inputs and the blower voltage as an output is nonlinear at an optimum oxygen excess ratio. Therefore, the set of data for the relation is obtained from multiple runs of the entire model at different currents and temperatures and used for a compensation of the effects.

4. Simulation and analyses

Simulations are performed to analyze the dynamic behavior of the stack along with the air supply, thermal system and the associated control strategies. Dynamics of water content in the membranes, temperature variations, oxygen excess ratio and system responses at load currents are discussed in the following sections. The empirical parameters and reference data for the models chosen are given in Table 1 ([6,10,12,13,26]). All models were coded by blocks given in MATLAB/Simulink.

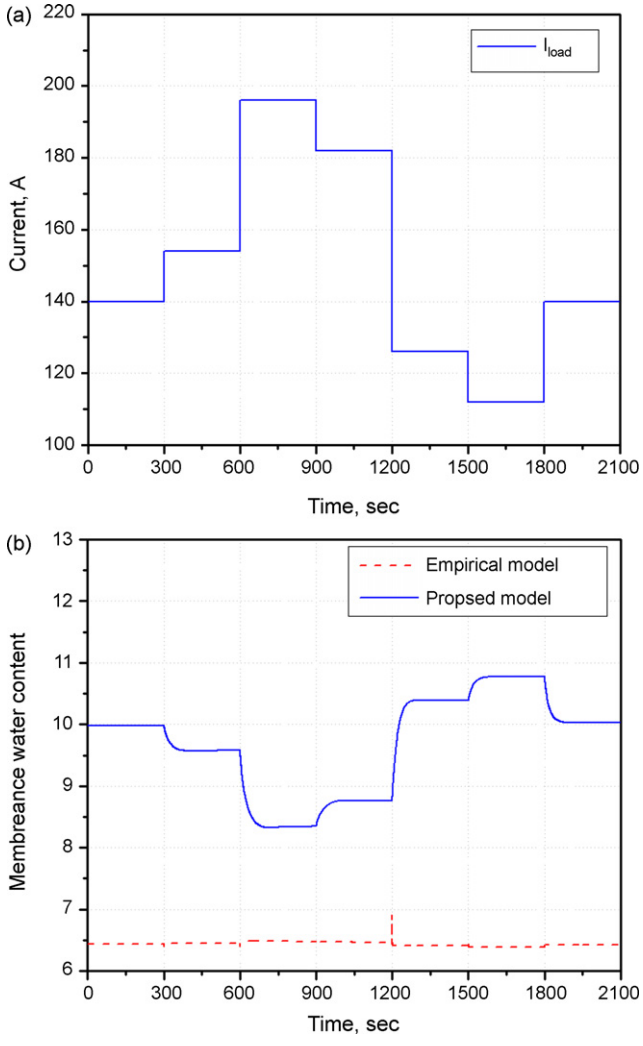

Fig. 3. (a) Current and (b) water content in the membrane.

Table 1
Simulation parameters

Fuel cell	
n	381
A_{fc}	0.028 m^2
Proton conducting model [12]	
b_{11}	0.5139
b_{12}	0.326
b_2	350
n_d	$f(C_{water})$
D_w	$f(T, C_{water})$
Gas transport model [10]	
D_{eff}	$f(P, T)$ m^2 s^{-1}
P_{sat}	$f(T)$
Electrochemical reaction model [6]	
P_0	1.0 bar
T_{ref}	353.15 K
E_{ref}	1.229 V
$A_{catl,eff}/A_{cell}$	$f(I, T, P_{o2})$
Thermal model [13]	
H_{gas}	$f(P, T)$
$C_{p_{gas}}$	$f(P, T)$
ρ_{gas}	$f(P, T)$
Fr	0.6
m_{res}	5
h_{rad}	5.897

	Thickness (m)	Density (kg m^{-3})	Heat conductivity (W m^{-1} K^{-1})	Specific heat (J kg^{-1} K^{-1})
Geometrical data for layers [26]				
Coolant channel	0.001	1400	52	935
Plate	0.001	1400	52	935
Gas channel	0.001	1400	52	935
GDL	0.0004	2000	65	840
Catalyst layer	0.000065	387	0.2	770
Membrane layer	0.000183	1967	0.21	1100

4.1. Water content in the membrane

Fig. 3 shows a comparison of the membrane water content between the empirical and the proposed model at a step load current. The membrane water content is a function of the water activity (Eq. (9)) that depends upon the saturated vapor pressure and vapor pressures of the cathode and anode sides. Hence, the saturated vapor pressure is a function of the temperature. Since the empirical model assumes a constant temperature of 353.15 K

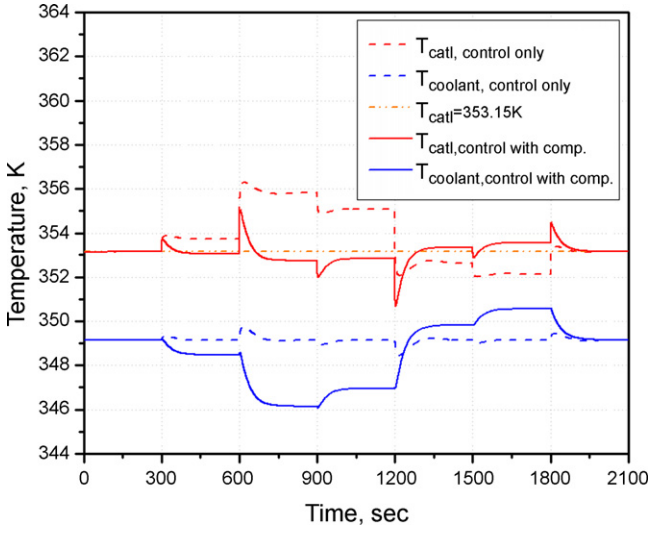

Fig. 4. Temperatures of the catalyst layer and coolant channel by the coolant flow controls.

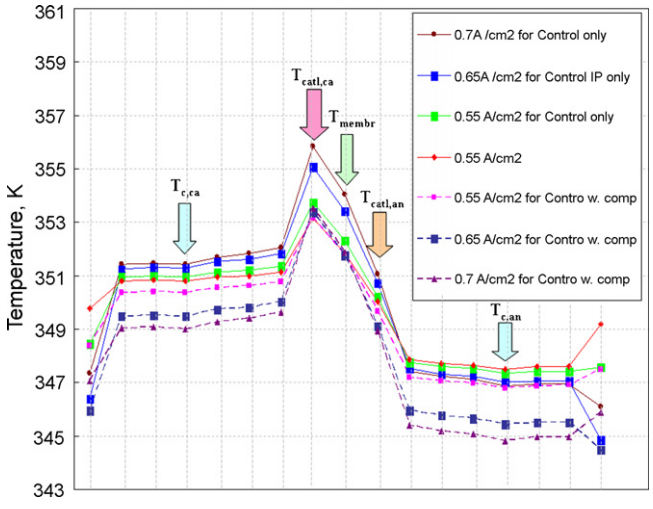

Fig. 5. Temperature variation in a cell depending on currents with and without the feed-forward of the disturbance.

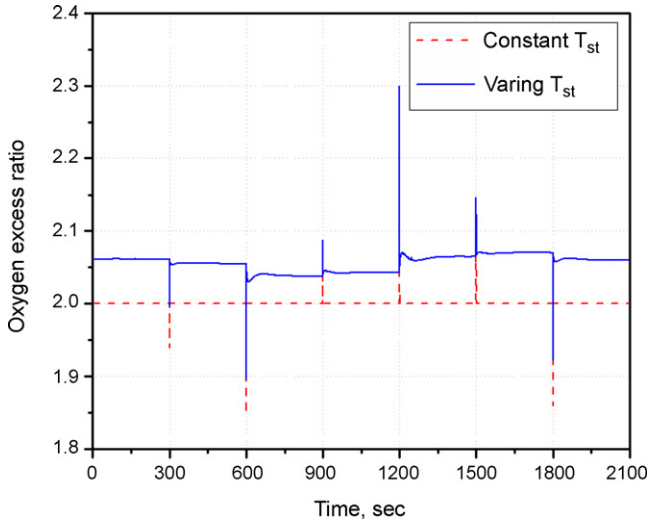

Fig. 6. Comparison of oxygen excess ratio at a constant and varying temperature.

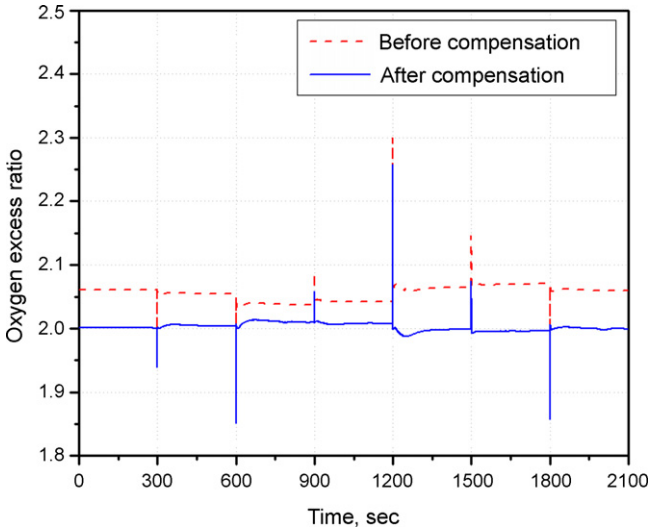

Fig. 7. Comparison of the oxygen excess ratio before and after temperature compensation.

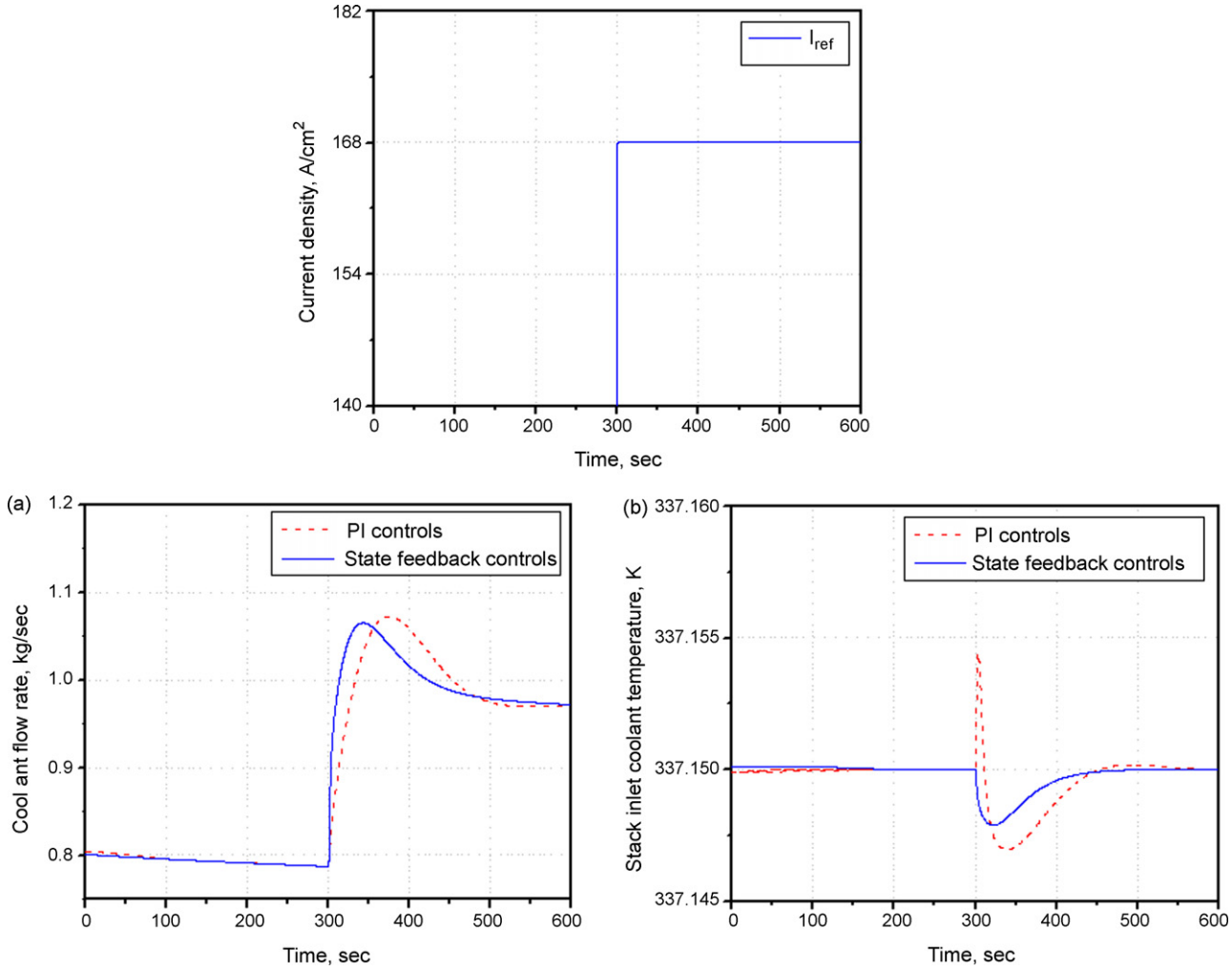

Fig. 8. Comparison of (a) coolant flow rate and (b) stack inlet coolant temperature with a given current step between PI controls and state feedback controls.

in the membrane, the vapor pressure likely correlates with the change of the load current, but no water transfer dynamics are involved.

Conversely, the variation of temperature and the change of water balance in the membrane dynamically influence the water content in the membrane. When the temperature in the coolant channels is maintained at 349.15 K, the temperature in the gas flow channel is higher than 349.15 K and the saturated vapor pressures in both of gas channels get increased. Consequently, the water activity and the water content become lower. The change of water balance is strongly influenced by the electro-osmotic force that is a function of the current (Eq. (4)). At a high load current, the elevated temperature of the stack leads to a high saturated vapor pressure and a low relative humidity on both sides of the cell as well as high electro-osmotic driving force. As a result, the membrane water content gets lower.

4.2. Temperature in the cell

Fig. 4 shows the temperature in the catalyst and coolant channel with and without the feed-forward of the disturbance. The actual temperature of the stack is usually measured at the stack outlet coolants on the anode and cathode sides and averaged. A reference temperature for the coolant control is set at 349.15 L.

When a multi-step current is applied to the stack, the temperature in the stack rapidly rises, particularly in the catalyst on the cathode side. The temperature rise is 3–7 K higher than the average temperature in the stack, where the coolant temperature is fully controlled at the reference temperature 349.15 K (see the dotted line in Fig. 4). It should be noted that the catalyst and membrane layers could be overheated and thereby damaged.

The difference in temperature in the layers can be reduced by a feed-forward (FF) of the disturbance to the coolant control loop that should reject excessive heat as quickly as possible. The transfer function of the disturbance is given in Eq. (35). The result of the control strategy proposed is illustrated in the Fig. 4 as a straight line, where the temperature of the catalyst layer is maintained close to 353.15 K. The coolant temperature shows the variation in the catalyst temperature. However, an instant rise in temperature cannot be fully suppressed because

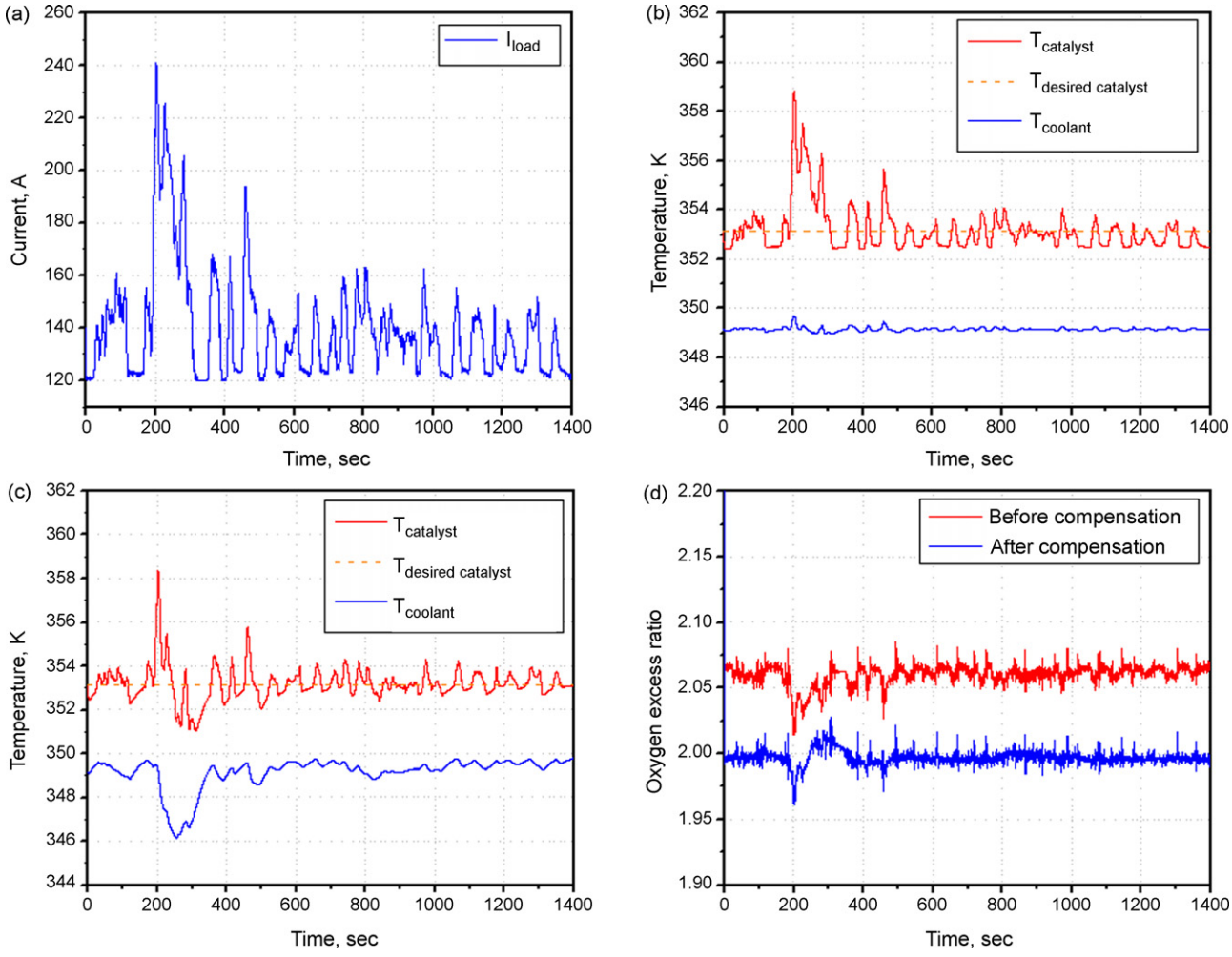

Fig. 9. (a) FUDS and a current profile with a base load of 120 A, (b) temperature of the catalysts and coolants without the FF, (c) temperature of the catalysts and coolants with the FF, and (d) oxygen excess ratio after a temperature compensation.

of the high thermal mass and large heat capacity of the stack. In addition, there is a steady state error caused by the temperature difference between the coolant channel measured and the catalyst layer. Nevertheless, the cell is cooled effectively and the exposure to heat on individual layers is minimized.

Fig. 5 shows the effects of the coolant controls on temperature distributions through the plane of a cell. As the amplitude of the current changes stepwise from 0.5 A to 0.55 A, 0.65 A and 0.7 A, the stack temperature becomes higher. When the feed-forward is applied, the overall stack temperature is lowered and the catalyst temperature is maintained at 353.5 K, which is significantly lower than before. Likewise, the maximum difference of the temperature between the catalyst on the cathode side and the coolant channel becomes 4 K lower than before. As a result, the cooling of the stack is more effective.

4.3. Oxygen excess ratio

Fig. 6 illustrates the oxygen excess ratio at constant and dynamically varying temperatures with a coolant flow control. Because of the change of pressure in the gas flow channel that is caused by variations in the stack temperature, the oxygen excess ratio is inversely changed as to the current change.

Fig. 7 shows a comparison of the oxygen excess ratio before and after compensation of the temperature influence on the air control loop. The compensation enables the oxygen excess ratio to be maintained at level 2, even though the current applied to the stack varies stepwise, which implies that the parasitic power at the blower is less.

4.4. Comparison of the PI and state feedback controls

Comparison between both controls shows that the parasitic power of the state feedback controls a multi-step current load is 5% less than that of the PI controller. However, the dynamic response is improved by the state feedback controls. In Fig. 8, step responses of two controls are simulated with the models discussed earlier. The output states are the coolant flow rate and the stack inlet coolant temperature. The rise time of the coolant flow rate by the state feedback controller, 6 s, is 4 times faster than that found with one PI controls. Likewise, the rise time of the stack inlet coolant temperature is 3 times faster than that of the PI controller.

Parasitic power is calculated as the sum of the electrical power necessary for driving the blower and the coolant pump. The control strategies with the proposed state feedback control require 100 kWs at the multiple step current, while that for the PI control loop requires 106 kWs.

The response of the state feedback control was compared with a conventional one by using a current profile obtained from a vehicle tested at the FUDS. Fig. 9 shows the simulation results for the two different control strategies at the load current. The peak temperature in the catalyst layer is 6 K higher than the working stack temperature by the control without the feed-forward (FF) control, even though the coolants are controlled around the set reference temperature shown in Fig. 9b. Fig. 9c shows the temperature of the catalyst and coolants with the FF of the disturbance. The peak of the temperature is similar to that of the others for the first 200 s, but is suppressed with a time delay associated with the closed-loop dynamic compare to Fig. 9b. The excursion duration of the catalyst temperature is decreased, and the heat energy imposed on the thin layers is reduced, which significantly reduces the heat stress on the layers. Correspondingly, the oxygen excess ratio shown in Fig. 9d is maintained at the optimum value compared to Fig. 6.

5. Conclusion

This article addresses the design of temperature control strategies for PEM fuel cells and their effects on dynamics and performance. We used a dynamic stack model and considered gas diffusion in the GDL, dynamic water balance in the membrane, temperature variation, and components of the air supply and thermal system. There are several major outcomes:

- Dynamic stack behavior was improved by adding dynamic water balance in the membrane and a partial pressure drop of reactants in the GDL and temperature distributions. The results show that distribution of the temperature through the plane is asymmetric and the temperature rise amounts to 3–7 K, which has the potential to damage the layers at a high current load. Therefore, proper control of the air and temperature might be required to ensure durability and efficiency;
- Most control strategies focused on optimization of the air supply system, where the working temperature in the fuel cell stack is presumed to be constant. However, we find that the oxygen excess ratio varies inversely with temperature. Thus, the ideal oxygen excess ratio necessary to prevent oxygen starvation cannot be maintained at the optimum value of 2;
- New control strategies proposed include a state feedback control with a feed-forward of the disturbance and a compensator for minimization of the temperature effect on the air flow rate. For the design of the temperature controller, the thermal circuit is approximated with a second order system. Classic PI and state feedback controls are used to compare the effectiveness of cooling. The results show that the temperature rise in the catalyst can be kept within an allowable value and duration. In addition, the oxygen excess ratio can be maintained at an optimal value by minimizing the influence of temperature variations in the gas flow channel. Consequently, the power consumption of the blower can be reduced by more than 15% by compensation, and 5% by the controlling bypass valve at a multi-step load profile. Using these techniques, the total parasitic power was reduced by approximately 7%.

Future work will assess other factors: (1) design of an observer for the temperature in the layers aiming at advanced controls and real-time diagnosis as well as the water content in the membrane and (2) optimization of the air and temperature controls with a real behavior of a humidifier.

Appendix A

$$A = \begin{bmatrix} -0.0245 & 0.0245 \\ 0.0243 & -0.0487 \end{bmatrix}, \quad B_{\mathrm{u}} = \begin{bmatrix} -0.3179 & 0 \\ 0.0089 & -1.1482 \end{bmatrix},$$

$$B_{\mathrm{w}} = \begin{bmatrix} 0.634 \times 10^{-5} \\ 0 \end{bmatrix}, \quad C = \begin{bmatrix} 1 & 0 \\ 0 & 1 \end{bmatrix}$$

$$A' = \begin{bmatrix} -0.0245 & 0.0245 & 0 & 0 \\ 0.0373 & -0.0488 & 0 & 0 \\ 1 & 0 & 0 & 0 \\ 0 & 1 & 0 & 0 \end{bmatrix},$$

$$B'_{\mathrm{u}} = \begin{bmatrix} -0.3179 & 0 \\ 0.0089 & -2.4756 \\ 0 & 0 \\ 0 & 0 \end{bmatrix},$$

$$Q = \begin{bmatrix} 10 & 0 & 0 & 0 \\ 0 & 1 & 0 & 0 \\ 0 & 0 & 0.01 & 0 \\ 0 & 0 & 0 & 0.01 \end{bmatrix},$$

$$R = \begin{bmatrix} 100 & 0 \\ 0 & 1 \end{bmatrix}$$

References

[1] W.C. Yang, B. Bates, N. Fletcher, R. Pow, Control challenges and methodologies in fuel cell vehicle development, SAE paper 98C054, 1998.
[2] F. Amir, G. Zhen, Int. J. Heat Mass Tranf. 48 (2005) 3891–3920.
[3] T. Nguyen, R.E. White, J. Electrochem. Soc. 140 (1993) 167–174.
[4] X. Ren, S. Gottesfeld, J. Electrochem. Soc. 148 (1) (2001) 87–93.
[5] R.L. Borup, J.R. Davey, F.H. Garzon, D.L. Wood, M.A. Inbody, J. Power Sources 163 (2006) 76–81.
[6] J.T. Pukrushpan, H. Peng, A.G. Stefanopoulou, Simulation and analysis of transient fuel cell system performance based on a dynamic reactant flow model, in: Proc. of the IMEXE'01, ASME International Mechanical Engineering Congress & Exposition, New Orleans, LA, 2002.
[7] G.H. Guvelioglu, H.G. Stenger, J. Power Sources 147 (1–2) (2005) 95–106.
[8] S. Um, C.Y. Wang, Computational fluid dynamics modeling of proton exchange-membrane fuel cells, J. Electrochem. Soc. 147 (2000) 4485–4493.
[9] L. Ma, D.B. Ingham, M.C. Pourkashanian, E. Carcadea, J. Fuel Cell Sci. Technol. 2 (4) (2005) 246–257.
[10] T.E. Springer, T.A. Zawodzinski, S. Gottesfeld, J. Electrochem. Soc. 138 (8) (1991) 2334–2342.
[11] Y. Shan, S.Y. Choe, J. Power Sources 145 (1) (2005) 30–39.
[12] M. Ceraolo, C. Miulli, A. Pozio, J. Power Sources 113 (2003) 131–144.
[13] S. Gurski, Cold start effects on performance and efficiency for vehicle fuel cell system, Master of Science Thesis, Virginia Polytechnic Institute and State University, 2002.
[14] M.J. Lampinen, M. Fomino, J. Electrochem. Soc. 140 (12) (1993) 3537–3546.
[15] J.C. Amphlett, R.M. Baumert, R.F. Mann, B.A. Peppley, P.R. Roberge, Performance modeling of the Ballard Mark IV solid polymer electrolyte fuel cell, J. Eletrochem. Soc. 142 (1) (1995) 9–15.
[16] S. Gelfi, A.G. Stefanopoulou, J.T. Pukrushpan, H. Peng, Proceedings of the American Control Conference, Denver, Colorado, 2003.
[17] R.T. Meyer, B. Yao, Modeling simulation of a modern PEM Fuel cell system, in: Proceedings of the Fuel Cell, Irvine, CA, June, 2006.
[18] Phoenix Design & Technologies, The PDAT Turbomix. http://www.padtinc.com/sales/fuelcell/turbomix/, March 2007.
[19] D.G. Kroger, Radiator Characterization and Optimization, SAE paper 840380, 1984.
[20] M. Grujicic, K.M. Chittajallu, E.H. Law, J.T. Pukrushpan, J. Power Energy 218A (2004), 487–450.
[21] A.D. Domenico, A. Miotti, M. Alhetairshi, Y.G. Guezennec, S.S.V. Rajagopalan, S. Yurkovich, Multi-variable control for an automotive traction PEM fuel cell system, in: Proc. of the 2006 American Control Conference, Minneapolis, Minnesota, 2006.
[22] P. Rodatz, G. Paganelli, L. Guzella, Optimization air supply control of a PEM fuel cell system, in: IEEE Proc. American Control Conference, 2003.
[23] A. Vahidi, A.G. Stefanopoulou, H. Peng, Model predictive control for starvation prevention in a hybrid fuel cell system, in: IEEE Proc. American Control Conference, 2004.
[24] B.D.O. Anderson, J.B. Moore, Optimal control: Linear Quadratic Methods, Prentice-Hall, NJ, USA, 1989.
[25] M. Grujicic, K. Chittajallu, J.T. Pukrushpan, Proc. Intl. Mech. Engrs. 218D (2004).
[26] M. Sundaresan, A thermal model to evaluate sub-freezing startup for a direct hydrogen hybrid fuel cell vehicle polymer electrolyte fuel cell stack and system, Ph.D. Thesis, Transportation Technology and Policy, UC Davis, 2004.